Supplementary information

Syngas production by photoreforming of formic acid with 2D $V_xW_{1-x}N_{1.5}$ solid solution as an efficient cocatalyst

Xiaoyuan Ye, Yuchen Dong, Ziying Zhang, Wengao Zeng, Bin Zhu, Tuo Zhang, Ze Gao, Anna Dai, and Xiangjiu Guan[*]

International Research Center for Renewable Energy, State Key Laboratory of Multiphase Flow in Power Engineering, Xi'an Jiaotong University, Xi'an 710049, China

Keywords: photocatalysis, syngas, formic acid, cocatalyst, solid solution.

[*] Corresponding author Email: xj-guan@mail.xjtu.edu.cn (Guan X. J.)

Experimental section

Preparation of VN_x sample

VN_x was produced by annealing the V_2O_5 precursor at 750 °C for 5 hours at a ramp rate of 1 °C min^{-1} at 5% NH_3/Ar atmosphere. Then, the product was washed via ultra-sonication in deionized water to remove salt. Afterwards, the product was washed in deionized water by ultrasonic for 30 minutes to dissolve the salt. Finally, it was filtered and freeze-dried to obtain VN_x samples.

Preparation of TiO_2-based and g-C_3N_4-based hybrid photocatalysts sample

TiO_2 (P25) was purchased from Sigma Andrich. g-C_3N_4 (denoted as CN) was obtained by calcination using urea as precursor [1]. $TiO_2/V_{0.1}W_{0.9}N_{1.5}$ and $CN/V_{0.1}W_{0.9}N_{1.5}$, were synthesized by simple physical mixing. Generally, photocatalyst (TiO_2 or CN) was mixed with 2D $V_{0.1}W_{0.9}N_{1.5}$ in 5 mL of ethanol absolute by sonicating for 1 hour and then stirring for 12 hours at room temperature. After that, the sample was vacuum-dried at 65 °C and collected. TiO_2/W_2N_3 and CN/W_2N_3 was prepared using the similar method described above.

Characterizations

The powder X-ray diffraction (XRD) patterns were obtained from a PANalytical X'pert MPD diffractometer operated at 40 kV and 40 mA using Ni-filtered Cu Kα irradiation (λ =1.5406 Å). Field-emission scanning electron microscopy (FESEM) images were observed by a JEOL JSM-7800 F instrument. The energy dispersive X-ray spectrometer (EDX) was carried by Oxford INCA instrument mounted on scanning electron microscope. Transmission electron microscopy (TEM) images were obtained from a transmission electron microscope (JEOL JEM-F200 (HR)) with an accelerating voltage of 200 kV, and elemental mapping over the selected region of the photocatalyst was conducted by an attached energy-dispersive X-ray spectrometer. The X-ray photoelectron spectra (XPS) were obtained on a Kratos Analytical Axis Ultra DLD instrument with a monochromatized Al Kα line source (150 W). All binding energies were referenced to the C 1s peak at 284.8 eV. Samples of powder were pressed into sheets by a tablet pressing machine. The ultraviolet photoelectron spectroscopy (UPS) was

measured on Thermo Fisher ESCALAB Xi+. The UV-vis absorption spectra (UV-vis) were measured on an Agilent Cary 5000 instrument equipped with a diffuse-reflectance accessory and with $BaSO_4$ as the reference. The photoluminescence spectra (PL) analysis was conducted on a PTI QuantaMaster 40 steady-state fluorescence spectrophotometer at room temperature with a solid-state sample. The *in situ* electron paramagnetic resonance (EPR) measurements were conducted by a Bruker A300-9.5/12. The samples were irradiated in the cavity of the EPR spectrometer with a Xe lamp. The inductively coupled plasma-mass spectrometry (ICP-MS) measurements were conducted by a NxeION 5000G (PerKinElmer).

Selectivity

In this work, when focusing only on reactants and generators, the photoreforming of FA could proceed via two distinct reactions: 1) $HCOOH \rightarrow H_2 + CO_2$; 2) $HCOOH \rightarrow H_2O + CO$. Thus, the selectivity of H_2 was calculated according to the equation: Selectivity (H_2) = 100% × $n(H_2)/(n(H_2) + n(CO))$. $n(H_2)$ and $n(CO)$ are the amount of H_2 generated and CO generated, respectively. Then the selectivity of CO was easy to calculate by the equation: Selectivity(CO) = 100%−Selectivity(H_2). In this paper, the selectivity refers to the selectivity of H_2, unless otherwise specified.

Inhibition experiments

In detail, 4 mg $CdS/V_{0.1}W_{0.9}N_{1.5}$ hybrid photocatalyst and 80 mL 4 M FA aqueous solution were mixed into a Pyrex glass cell (105 mL) with a side window for external light incidence and kept ultrasonic for at least 10 min. Then, 6.67 mmol EDTA disodium (Na_2EDTA) or 5 mL of isopropanol was added to the above solution and stirred for 30 minutes. Subsequently, the reaction system was deoxygenated with Ar for at least 20 min. Finally, the inhibition experiments were performed by a similar step (**Method: Evaluation of photocatalytic performance**).

Calculation

Spin-polarized density functional theory (DFT) calculations were employed using the Vienna Ab-initio Simulation Package (VASP) [2,3]. The projector-augmented wave (PAW) method was adopted to describe the nuclei-electron interactions[4,5], with a 500 eV cut-off plane wave basis set. The exchange and correlation effects were described within the generalized

gradient approximation (GGA) in the Perdew-Burke-Ernzerhof form [6]. Gaussian smearing with a width of 0.05 eV was used for electron smearing. All the calculations included BJ-damping DFT-D3 dispersion correction [7,8] with convergence thresholds of 10^{-5} eV and 0.02 eV/Å for energy and force, respectively. The catalysts were represented by 5-atom-layered slab structures, containing 18 metal atoms and 27 N atoms each, and the V-doped structure was constructed by substituting 3 W atoms with V atoms. A vacuum layer of 15 Å along the *z*-axis was introduced into the slab models, to avoid the spurious interaction of neighboring supercells. A 3×3×1 *k*-point mesh was adopted for geometric optimization, and line-mode *k*-points along $\Gamma - \mathrm{M} - \mathrm{K} - \Gamma$ path was used for band structure and density of state (DOS) calculations.

Figure and Table

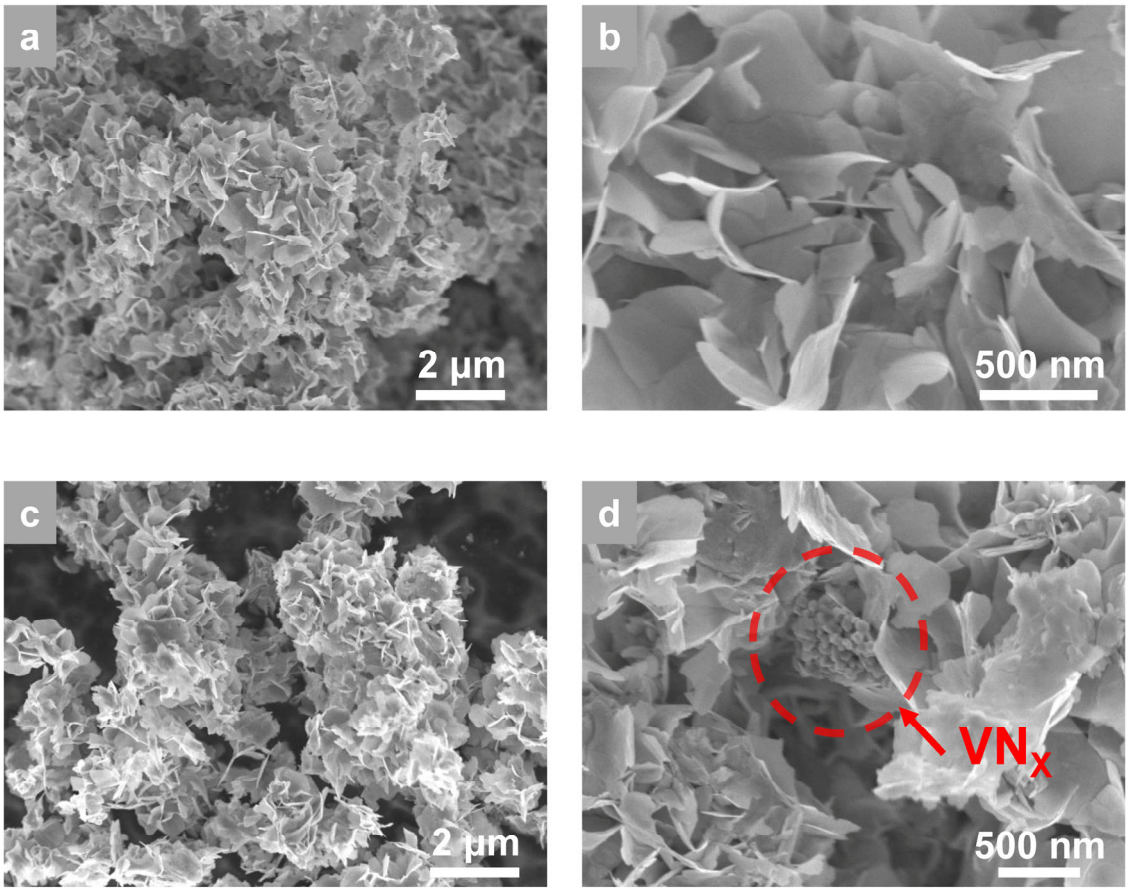

Fig. S1 SEM images.
(a) and (b) $V_{0.1}W_{0.9}N_{1.5}$ solid solution samples; (c) and (d) $V_{0.2}W_{0.8}N_{1.5}$ samples.

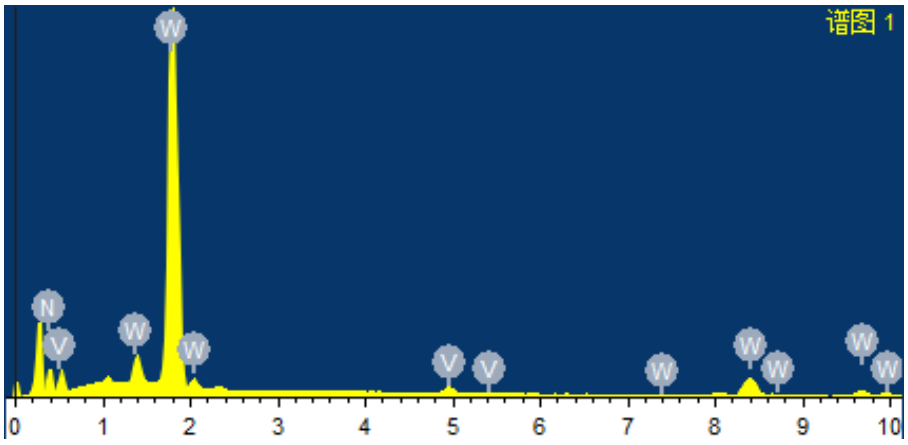

Fig. S2 EDS spectrum of $V_{0.1}W_{0.9}N_{1.5}$ solid solution sample.

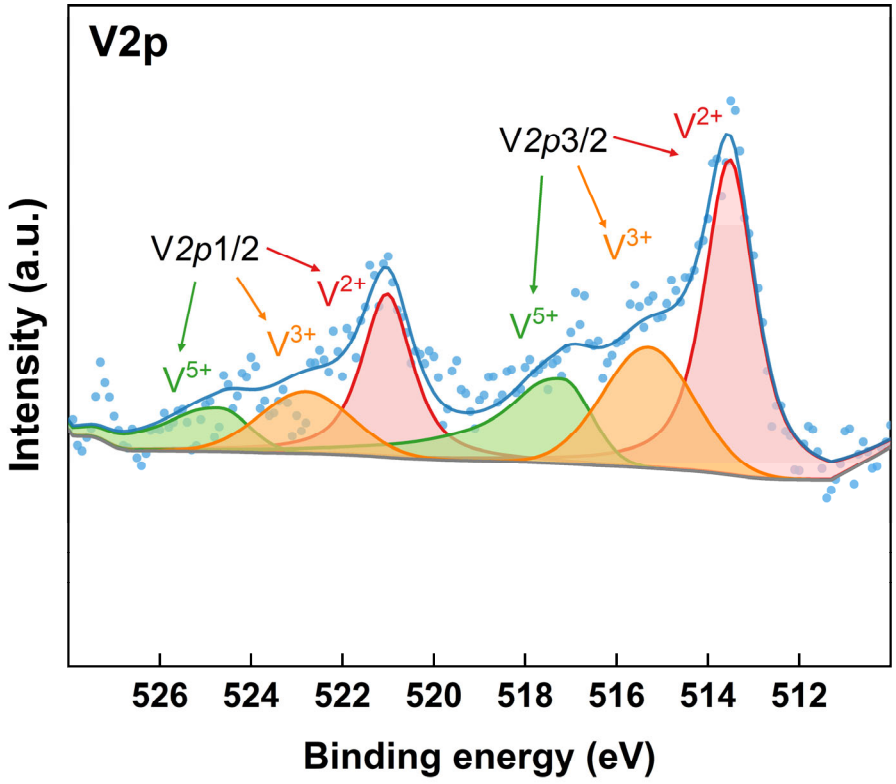

Fig. S3 Peak fits to high-resolution XPS V 2p spectra of $V_{0.1}W_{0.9}N_{1.5}$ sample.

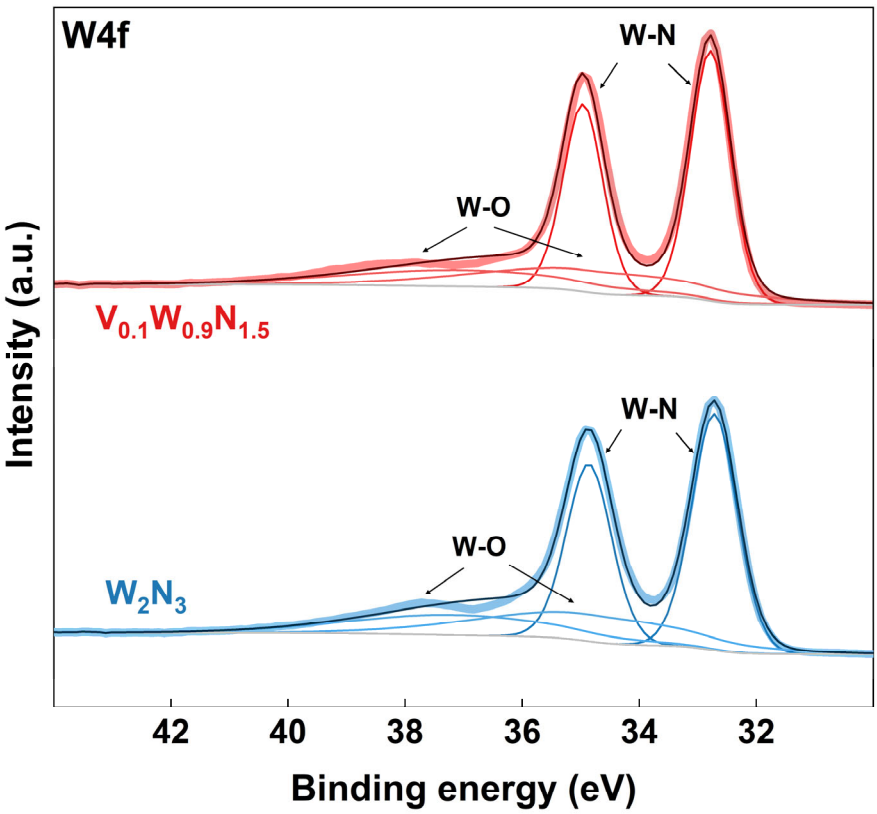

Fig. S4 Peak fits to high-resolution XPS W 4f spectra of W_2N_3 and $V_{0.1}W_{0.9}N_{1.5}$ sample.

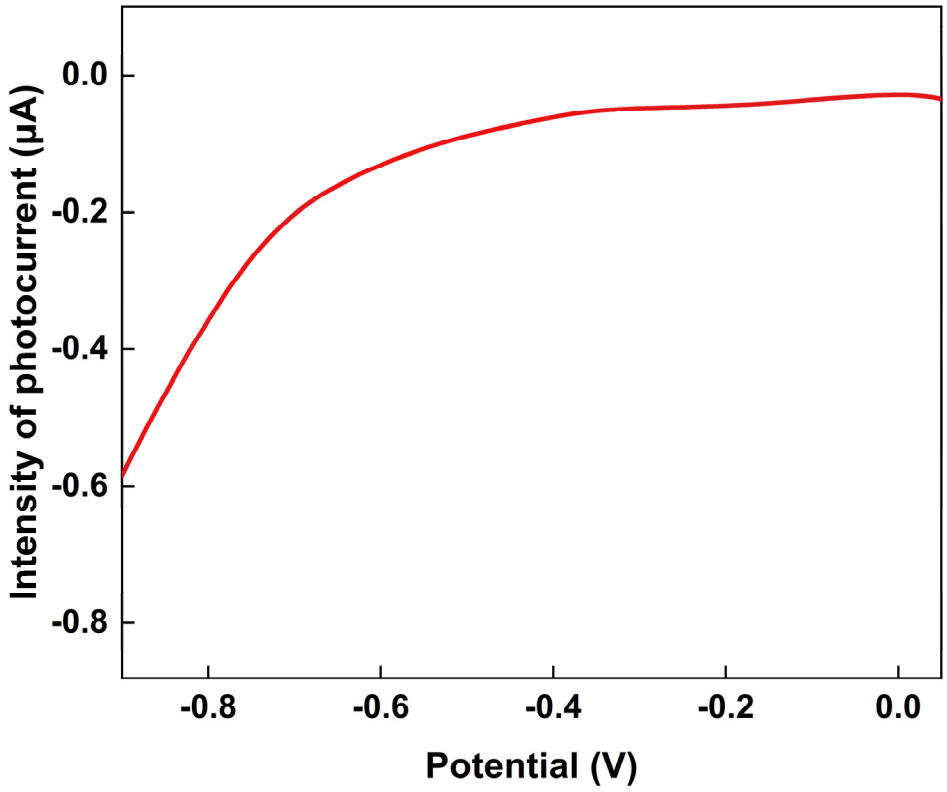

Fig. S5 Chopped-light linear sweep voltammetry (LSV) data for $V_{0.1}W_{0.9}N_{1.5}$ at a scan rate (V/s) of 0.01, and a light-chop of every 2 seconds.

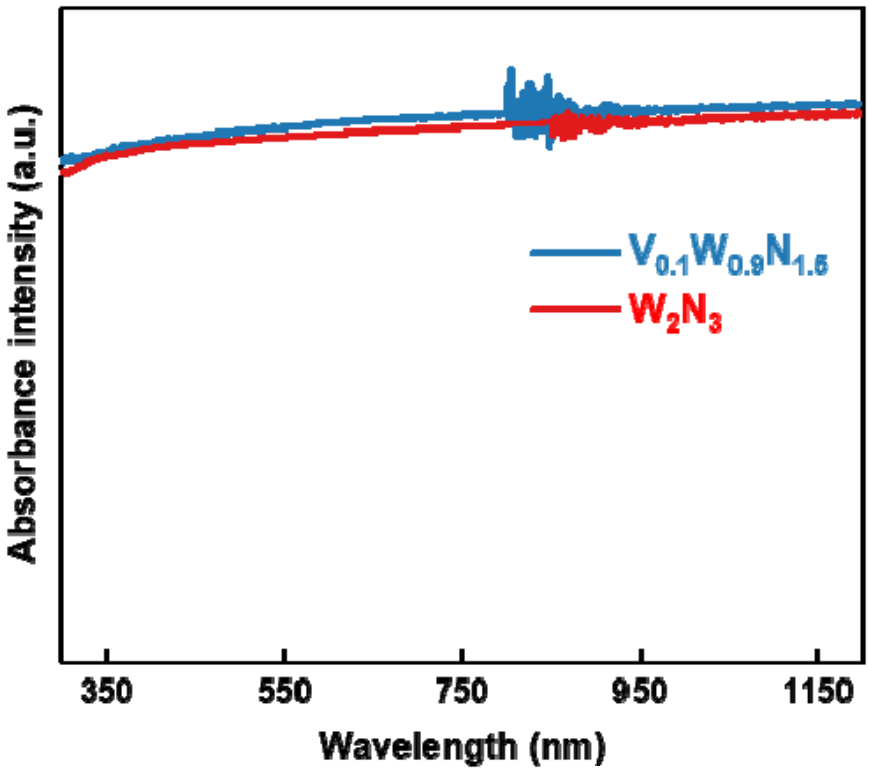

Fig. S6 UV-vis spectra of W_2N_3 and $V_{0.1}W_{0.9}N_{1.5}$.

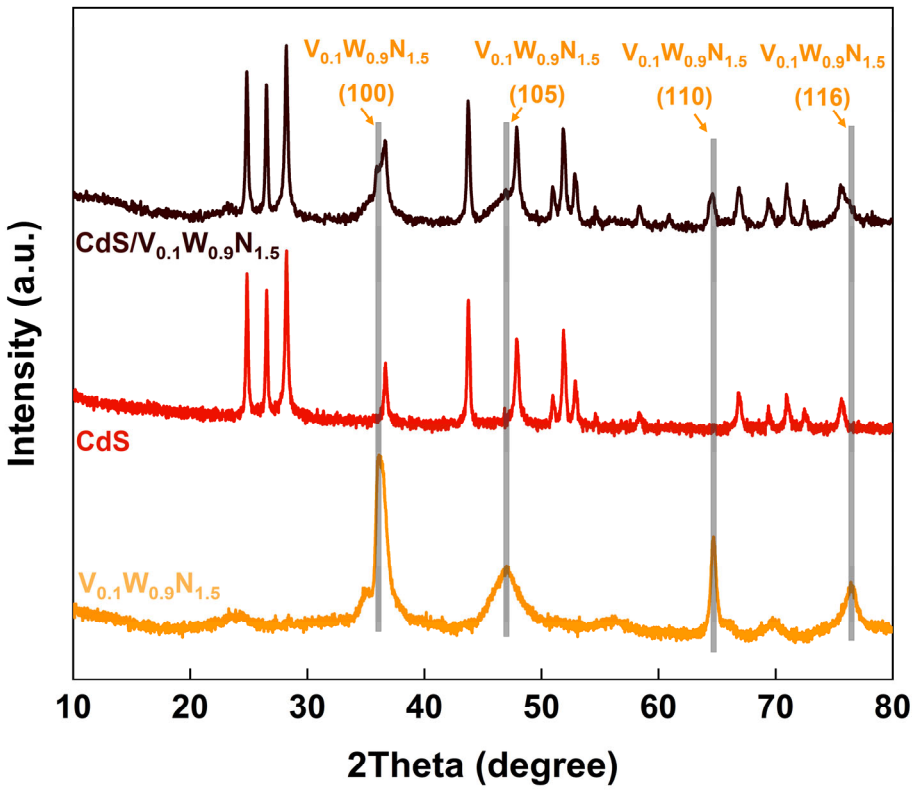

Fig. S7 XRD pattern of $V_{0.1}W_{0.9}N_{1.5}$, CdS, and $CdS/V_{0.1}W_{0.9}N_{1.5}$.

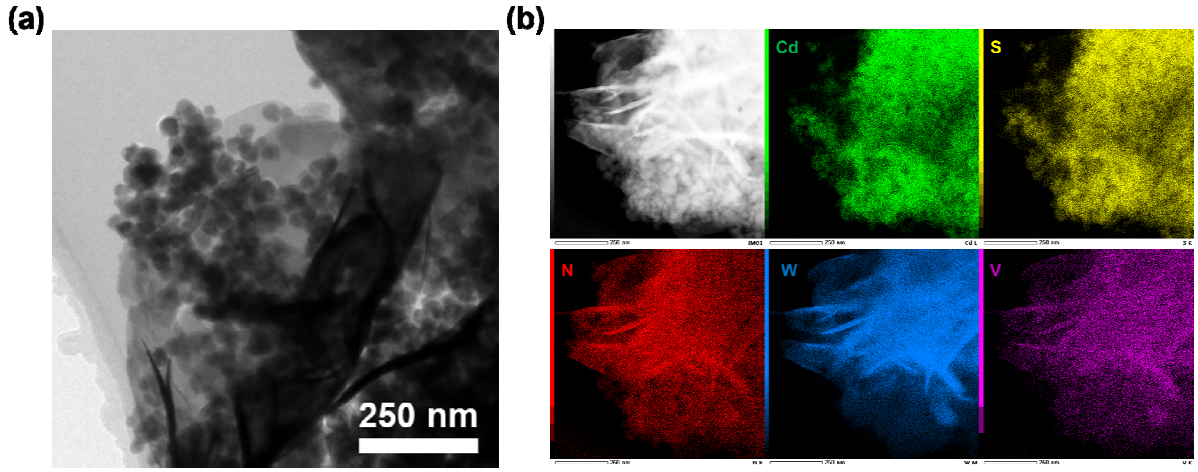

Fig. S8 (a) TEM image of $CdS/V_{0.1}W_{0.9}N_{1.5}$ hybrid photocatalyst; (b) STEM image and EDS mapping of $CdS/V_{0.1}W_{0.9}N_{1.5}$ hybrid photocatalyst.

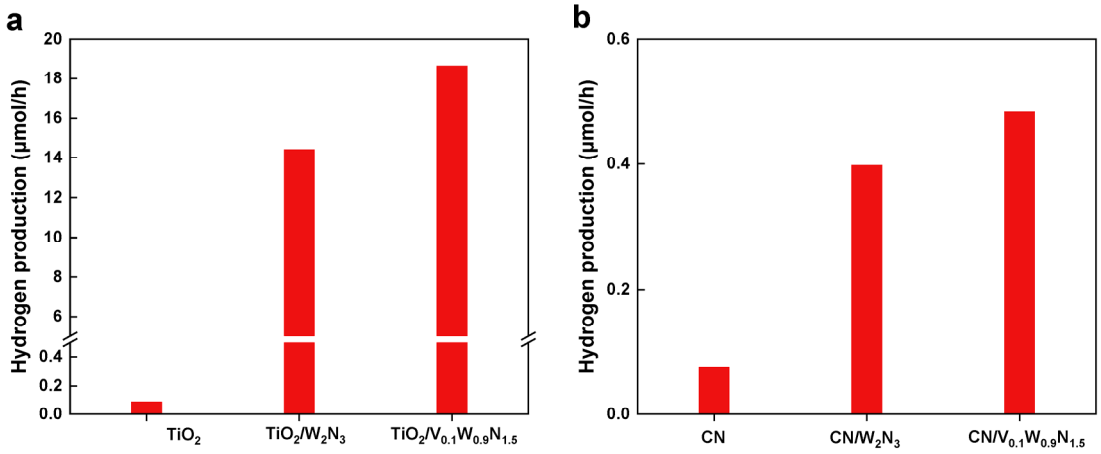

Fig. S9 Performance of photoreforming of FA with TiO_2 (a) and g-C_3N_4 (b) as photocatalysts and the $V_xW_{1-x}N_{1.5}$ as cocatalysts (All experiments in Fig. S9 were conducted in 1 M FA aqueous solution (80 mL) with 4 mg of catalyst under simulated sunlight.).

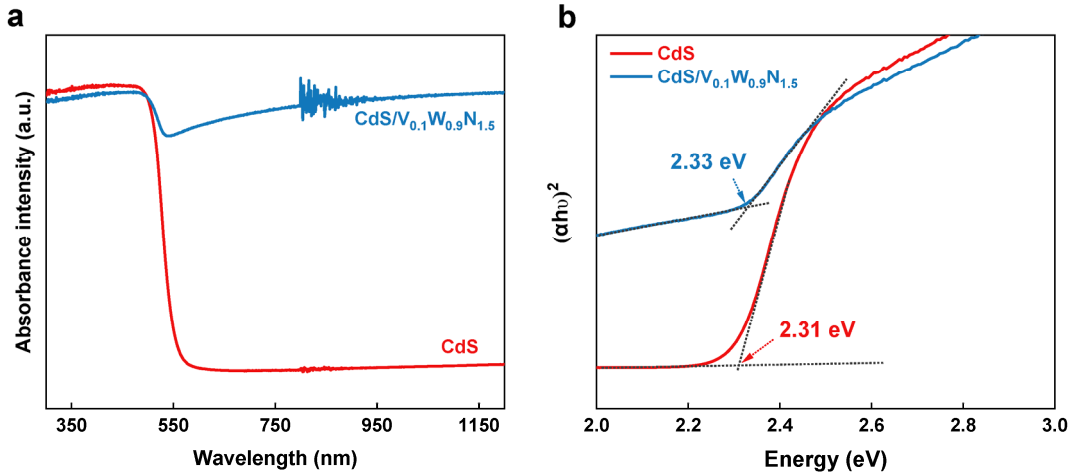

Fig. S10 (a) UV-vis spectrum of CdS and $CdS/V_{0.1}W_{0.9}N_{1.5}$ hybrid; (b) plots of $(\alpha hv)^2$ versus energy (hv) for the band gap of CdS and $CdS/V_{0.1}W_{0.9}N_{1.5}$ hybrid.

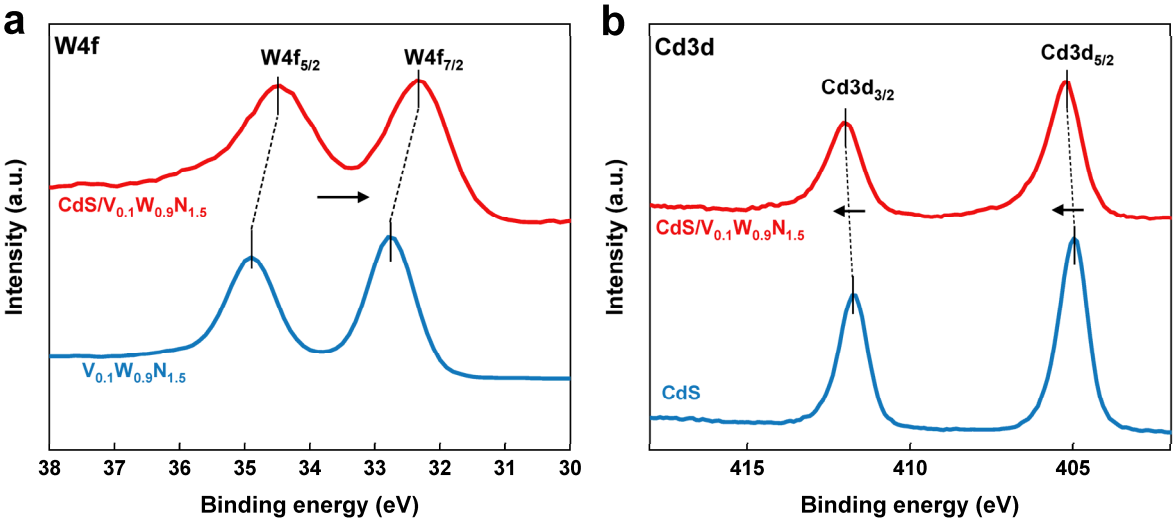

Fig. S11 (a) High-resolution XPS W 4f spectra of $V_{0.1}W_{0.9}N_{1.5}$ and $CdS/V_{0.1}W_{0.9}N_{1.5}$; (b) high-resolution XPS Cd 3d spectra of CdS and $CdS/V_{0.1}W_{0.9}N_{1.5}$.

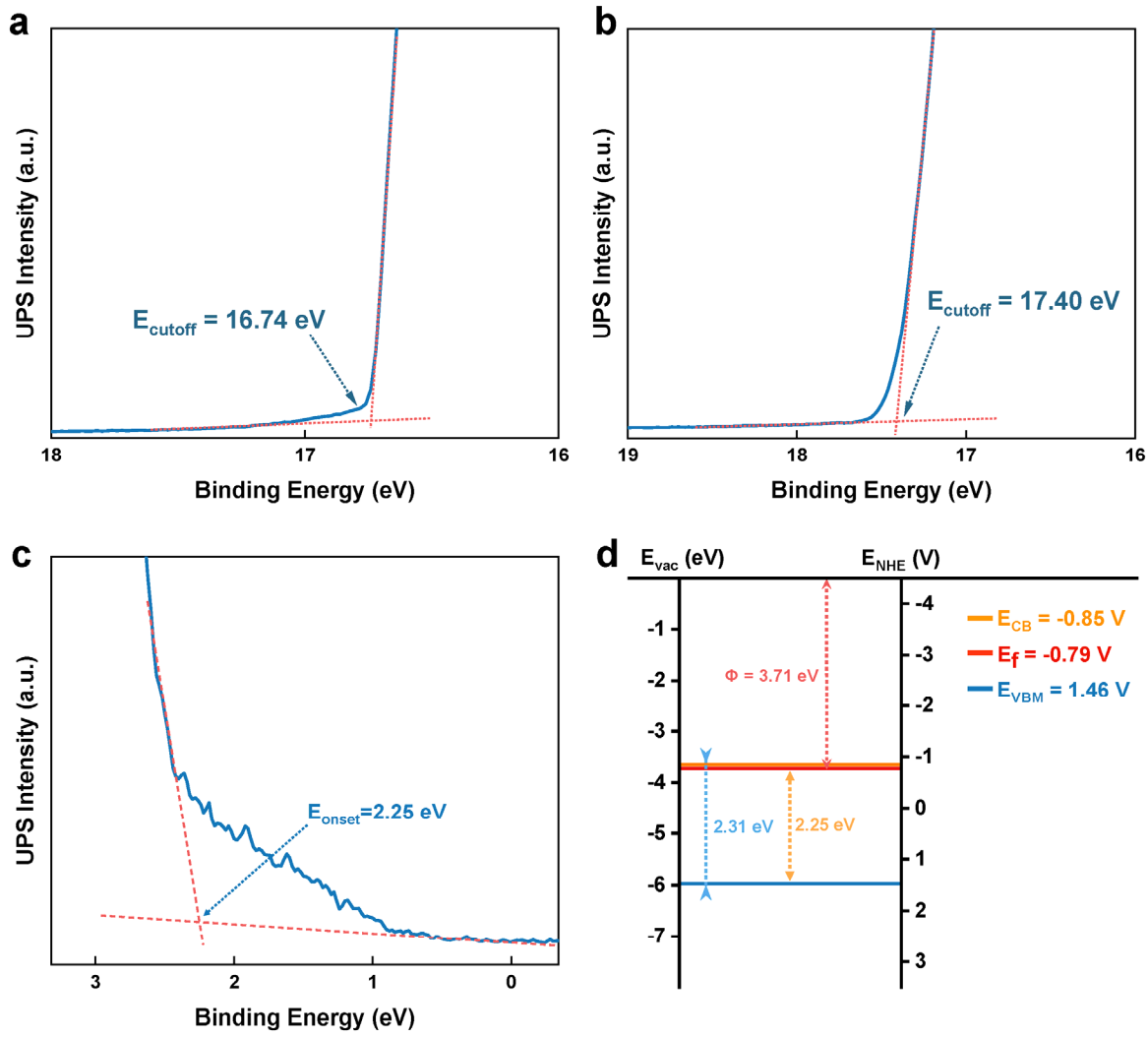

Fig. S12 Cutoff energy regions of UPS spectrum

(a) $V_{0.1}W_{0.9}N_{1.5}$; (b) CdS; (c) onset energy regions of CdS nanoparticle; (d) band edge positions of CdS nanoparticle.

Work function:

The work function (Φ = 21.22 eV–(E_{cutoff}–E_f)) values of $V_{0.1}W_{0.9}N_{1.5}$ and CdS were determined as 4.48 and 3.71 eV, respectively.

CdS band structure:

The CdS band structure was analyzed by UPS data and the results are showed in Fig. S12. First, the band gaps were calculated from UV-vis spectra by the reported formula: (αhv) n = B ($hv - E_g$), where h is the Planck constant, v is the frequency of photon, E_g is the band gap and B is a constant. The n factor is equal to 2 for CdS with the direct transition band gap. As shown in the plots (Fig. S10b) of $(\alpha hv)^2$ versus energy (hv), the linear part of the plot is extrapolated to the x-axis, and the intercept in x-axis corresponds to the band gap (E_g) of 2.31 eV. Then, ultraviolet photoelectron spectroscopy (UPS) was performed to verify the position

of E_f and valence band (VB) (Fig. S12d). The work function (Φ = 21.22 eV–(E_{cutoff}–E_f)) and E_f-VBM (VBM: the VB maximum) values were determined as 3.71 and 2.25 eV, respectively. As shown in Fig. S12(d), the E_f value is –3.71 eV versus vacuum (–0.79 V versus NHE) and the VBM can be determined as –5.96 eV versus vacuum (1.46 V versus NHE). Finally, the conduction band potential (ECB) can be calculated as –0.85 V versus NHE by the formula $E_{CB} = E_{VB} - E_g$. These results indicate that the holes of CdS have a sufficient oxidation ability to translate HCOO– to $CO_2^{\bullet-}$ or CO_2 [9].

Table S1 Weight percentages of V element for different $V_xW_{1-x}N_{1.5}$ samples.

Sample	$V_{0.02}W_{0.98}N_{1.5}$	$V_{0.1}W_{0.9}N_{1.5}$	$V_{0.2}W_{0.8}N_{1.5}$
V(wt%)	0.34	1.98	4.22

The result is calculated based on the V concentration in the sample obtained in the inductively coupled plasma-mass spectrometry (ICP-MS) test.

Table S2 Photocatalytic activity of different samples of catalysts.

Catalyst	H_2 production/(μmol·h^{-1})	CO production/(μmol·h^{-1})	Selectivity/%	H_2/CO_2
CdS	26.67 ±5.06	29.42 ± 5.58	47.55 ± 0.49	1.98
CdS/W_2N_3	107.55 ± 1.11	22.95 ± 0.24	82.42 ± 0.54	2.83
CdS/$V_{0.02}W_{0.98}N_{1.5}$	162.24 ± 3.21	36.32 ± 0.72	81.71 ± 0.34	3.42
CdS/$V_{0.1}W_{0.9}N_{1.5}$	184.04 ± 10.94	39.47 ± 2.35	82.34 ± 0.76	3.46
CdS/$V_{0.2}W_{0.8}N_{1.5}$	106.84 ± 4.98	27.21 ± 1.27	79.70 ± 0.66	3.48
CdS/VN_x	8.97 ± 0.22	5.24 ± 0.13	63.14 ± 0.34	2.63
W_2N_3	no detected	no detected	n/a	n/a
$V_{0.1}W_{0.9}N_{1.5}$	no detected	no detected	n/a	n/a
No catalyst	no detected	no detected	n/a	n/a
CdS/$V_{0.1}W_{0.9}N_{1.5}$[a]	no detected	no detected	n/a	n/a
CdS/$V_{0.1}W_{0.9}N_{1.5}$[b]	no detected	no detected	n/a	n/a
CdS/$V_{0.1}W_{0.9}N_{1.5}$[c]	30.21 ± 6.89	trace[d]	~100[e]	11.82

All experiments were conducted in 80 mL 1 M FA aqueous solution for 4 h irradiation at room temperature. A sample of catalysts with 4 mg was used during the photocatalytic reaction. [a] The experiment was carried out in the dark. [b] Only pure water was used as reaction substrate. [c] Only pure FA (98 wt.%) was used as reaction substrate. [d] trace: lower than reliable detection limit; [e] according to the presence of CO in trace amounts, it is believed that the selectivity of hydrogen is close to 100%. Under pure FA conditions, the selectivity was almost 100%, probably due to the higher concentration of H^+, which favors the occurrence of HER.

Table S3 the concentration of Cd element in the reaction solution.

Sample	CdS	$CdS/V_{0.1}W_{0.9}N_{1.5}$
Cd (ug/L)	5272.83	3820.45

All experiments were carried out in an 80 mL 4 M FA aqueous solution, using 4 mg of catalyst, and exposed to simulated sunlight for 12 hours. The concentration of Cd element in the reaction solution was determined using ICP-MS.

Reference

[1] A. Dai, Z. Huang, L. Tian, Z. Zhang, X. Guan, L. Guo. Phenyl-incorporated carbon nitride photocatalyst with extended visible-light-absorption for enhanced hydrogen production from water splitting. *J. Colloid Interface Sci.*, 622 (2022) 494–502.

[2] G. Kresse, J. Furthmüller. Efficiency of ab-initio total energy calculations for metals and semiconductors using a plane-wave basis set. *Computational Materials Science*, 6 (1996) 15–50.

[3] G. Kresse, J. Furthmüller. Efficient iterative schemes for ab initio total-energy calculations using a plane-wave basis set. *Physical review B*, 54 (1996) 11169.

[4] P.E. Blöchl. Projector augmented-wave method. *Physical Review B*, 50 (1994) 17953.

[5] G. Kresse, D. Joubert. From ultrasoft pseudopotentials to the projector augmented-wave method. *Physical review B*, 59 (1999) 1758.

[6] J.P. Perdew, K. Burke, M. Ernzerhof. Generalized gradient approximation made simple. *Physical Review Letters*, 77 (1996) 3865.

[7] S. Grimme, J. Antony, S. Ehrlich, H. Krieg. A consistent and accurate ab initio parametrization of density functional dispersion correction (DFT-D) for the 94 elements H-Pu. *The Journal of Chemical Physics*, 132 (2010) 154104.

[8] S. Grimme, S. Ehrlich, L. Goerigk. Effect of the damping function in dispersion corrected density functional theory. *Journal of Computational Chemistry*, 32 (2011) 1456–1465.

[9] L. Yuan, M.Y. Qi, Z.R. Tang, Y.J. Xu. Coupling strategy for CO_2 valorization integrated with organic synthesis by heterogeneous photocatalysis. *Angew. Chem. Int. Ed. Engl.*, 60 (2021) 21150–21172.